ACS OMEGA

Open Access

http://pubs.acs.org/journal/acsodf

Article

Ophiorrhiza mungos-Mediated Silver Nanoparticles as Effective and Reusable Adsorbents for the Removal of Methylene Blue from Water

Aklima A Akhi, Abid Hasan, Nakshi Saha, Sabbir Howlader, Sabonty Bhattacharjee, Kamol Dey, A. K. M. Atique Ullah, Farhana Rumzum Bhuiyan, Ashok Kumar Chakraborty, Umme Sarmeen Akhtar, Md. Aftab Ali Shaikh, Benu Kumar Dey,* Samiran Bhattacharjee,* and Sumon Ganguli*

Cite This: *ACS Omega* 2024, 9, 4324−4338

Read Online

ACCESS | Metrics & More | Article Recommendations | Supporting Information

ABSTRACT: Green synthesis of silver nanoparticles (AgNPs) using a plant extract has attracted significant attention in recent years. It is found as an alternative for other physicochemical approaches because of its simplicity, low cost, and eco-friendly rapid steps. In the present study, *Ophiorrhiza mungos* (*Om*)-mediated AgNPs have been shown to be effective bioadsorbents for methylene blue (MB) dye removal (88.1 ± 1.74%) just after 1 h at room temperature in the dark from an aqueous medium for the first time. Langmuir and Freundlich isotherms fit the experimental results having the correlation coefficient constants R^2 = 0.9956 and R^2 = 0.9838, respectively. From the Langmuir fittings, the maximum adsorption capacity and adsorption intensity were found to be 80.451 mg/g and 0.041, respectively, indicating the excellent performance and spontaneity of the process. Taking both models under consideration, interestingly, our findings indicated a fairly cooperative multilayer adsorption that might have been governed by chemisorption and physisorption, whereas the adsorption kinetics followed the pseudo-second-order kinetics mechanism. The positive and low values of enthalpy (ΔH^0 = 4.91 kJ/mol) confirmed that adsorption is endothermic and physical in nature; however, the negative free energy and positive entropy value (ΔS^0 = 53.69 J/mol K) suggested that the adsorption is spontaneous. The biosynthesized adsorbent was successfully reused up to the fifth cycle. A proposed reaction mechanism for the adsorption process of MB dye onto *Om*-AgNPs is suggested. The present study may offer a novel finding such as an effective and sustainable approach for the removal of MB dye from water using biosynthesized *Om*-AgNPs as reusable adsorbents at a comparatively faster rate at a low dose for industrial applications.

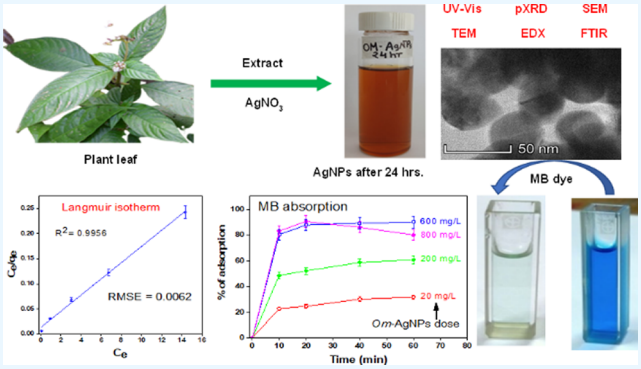

INTRODUCTION

Green bionanotechnology plays an important role, mainly focusing on more sustainable and safer products by reducing waste and escaping the use of hazardous chemicals. Hence, researchers desired to develop an alternative way for the production of metal nanoparticles, and that has prompted them to switch to environmentally friendly techniques named "green synthesis". The magical ability to develop bioactive secondary metabolites is a gift from nature to the plant; so, scientists have used plant extracts that contain different phytoconstituents for the large-scale production of bioinspired metal nanoparticles.[1] Secondary metabolites (e.g., terpenes, phenolics, alkaloids, thionins, etc.) basically originated from primary metabolites.[2] They have been considered to be attention-grabbing and widely used due to their multiplicity in their structure and their strength as a reducing agent, subsequently stabilizing and capping nanoparticles during synthesis.[3]

Among the metal nanoparticles, silver nanoparticles (AgNPs) as a catalyst[4,5] in wastewater treatment, making water filters,[6] in biosensors,[7] and in the medical field as a therapeutic agent[8] have recently gained substantial attention due to their unique properties. The electrical, optical, and thermal properties of AgNPs can be tuned into products for a variety of uses, from chemosensors and photovoltaics to biological applications.[9] Taken together, AgNPs are considered as widely studied nanomaterials in the degradation of organic dyes and, therefore, have been chosen for our investigation. For instance, AgNPs were synthesized using *Gmelina arborea* extract,[10] *Achillea millefolium* L. extract,[11] and *Hibiscus*

Received: August 14, 2023
Revised: December 23, 2023
Accepted: December 29, 2023
Published: January 15, 2024

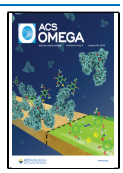

sabdariffa L. extract[12] to examine their catalytic properties. In addition, AgNPs were also synthesized using plants to examine their antimicrobial, antioxidant, antibiofilm, anticoagulant, anticancer, wound-healing activities, and so forth.[13] Furthermore, AgNPs are utilized in the synthesis of industrially needed compounds in pharmaceuticals, agrochemicals, and their intermediates.[4] In consequence, very recently, we have reported on the formation of AgNPs with 17−26 nm in size using the same plant of *Ophiorrhiza* genus with excellent antibacterial and antifungal properties.[14]

On the one hand, the global clothing industry is considered one of the leading industries in the world, employing tens of millions of workers worldwide.[15] According to recent estimates, there were over 150 billion clothing items supplied in 2017, and by 2030, manufacturing is expected to rise by 63% to fulfill the demand from a growing global population.[15] Around 90 million metric tons of solid waste is predicted to be produced yearly by the sector, even at the present output levels.[15] Note that Bangladesh has approximately 7000 factories in textile sector which mainly manufacture readymade garments, woven, and knitwear.[16] Textile industries use a huge amount of dyes to provide classic texture to fabric materials. Various kinds of dyes (e.g., acid dyes, basic dyes, mordant dyes, etc.) are used in the textile dying industries for garment production.[17] MB is the most used dye that is highly soluble in water. MB is a notable cationic dye used in the textile sector for a wide range of applications. MB can induce eye burn, consequently leading to permanent damage of the eyes in both human and aquatic animals. Typically, cationic dyes, like MB, cause huge environmental pollution as well as impose a serious threat to living bodies.[18]

On the other hand, among the dye removal pathways, adsorption is a less expensive and the most acceptable technique than common effluent treatments to reduce the concentration of dissolved dyes from aqueous solutions.[8] When compared to other methods, adsorption is a preferable choice on account of its ease of design and operation, accessibility, effectiveness, immunity to harmful compounds, and low cost of course.[11] Therefore, the adsorptive removal of MB dye has been investigated over various Ag-based nanocomposites such as AgNPs deposited on graphene oxide,[19] AgNPs-loaded chitosan (AgCS nanocomposite),[20] AgNPs/GG (Guar Gum)/polyacrylic acid nanocomposite,[21] and Kaolin-supported AgNPs composite.[22] Moreover, activated carbon-loaded titanium dioxide nanocomposites,[23] nitrogen-rich biomass-derived carbon adsorbents,[24] bismuth oxyhalide solid solution,[25] metal oxide nanostructures,[26] metal oxide/biochar materials,[27] and poly(ethylene glycol)-modified magnetite nanostructures[28] have been reported to remove different dyes. However, it is noticeable that preparing nanocomposites required several preparative steps and external chemical compounds.[19−22] For instance, Kaolin-supported AgNPs showed substantial adsorption efficiency (98%), while external chemicals such as sodium borohydrate ($NaBH_4$) were used with the catalyst for the adsorptive removal of MB dye.[22]

Although green synthesis of AgNPs was available for different applications, as mentioned earlier, nevertheless, after going through much literature, very little is known regarding dye removal through the adsorption pathway of using green-synthesized AgNPs, except in only a few recent literature.[20,29,30] Sultan et al.[20] reported the synthesis of AgNPs using *L. lucium* leaf extract and incorporated on the chitosan surface. The AgNPs-loaded chitosan nanocomposites showed 70% MB dye removal using ultrasound-assisted adsorption. Recently, Gowda et al.[29] described the biosynthesis of UL-AgNPs using *Urena lobata* (*UL*) leaf extract for the adsorption of MB dye. *UL*-AgNPs showed an effective adsorbent (87.5% MB removal) with the maximum adsorption capacity of 218.95 mg/g; however, the mechanism involved in the process was unexplored in detail.[29] In another report, *Salvinia molesta* (*Sm*) AgNPs showed almost 98% MB removal with 121.04 mg/g of adsorption capacity, while the synthesis time was long (72 h).[30]

Thus, a simple preparation route of AgNPs using plant extract with a high breaking down capacity of organic dyes from aqueous medium will be highly desirable. The *Ophiorrhiza* genus plant has been reported to contain various potential secondary metabolites such as alkaloids, flavonoids, steroids, and terpenoids, as shown in the Supporting Information (S1). As described above, highly stable AgNPs were synthesized through an eco-friendly approach using aqueous leaf extracts of three *Ophiorrhiza* species with excellent size-dependent antimicrobial activity.[14] We have shown that biomolecules play a crucial role in controlling the particle size of AgNPs, assisting in the reduction of Ag^+ to Ag^0 along with the capping and stabilizing agents of nanoparticles. Using the *Ophiorrhiza* genus plant extracts, the smallest AgNPs were attained from *Ophiorrhiza mungos* (17 nm), while *Ophiorrhiza harrisiana* and *Ophiorrhiza rugosa* produced the largest AgNPs (22 and 26 nm, respectively).[14] Taken together, within this line, in this study, we demonstrated that the *Om*-mediated AgNPs, *Om*-AgNPs, are highly effective and reusable nanoadsorbents in removing MB dye from water. The adsorption capacity was evaluated using different established isotherm and kinetic models which may help to design reactors for industrial application. A plausible reaction mechanism by the *Om*-AgNPs material is proposed. To our knowledge, using biosynthesized *Om*-AgNPs for the removal of MB dye has not been previously reported. This adsorbent could be used to degrade other dye molecules that could lead to a pathway in real wastewater treatment.

MATERIALS AND METHODS

Materials. Silver nitrate ($AgNO_3$, ≥99.0%) and methylene blue (MB) ($C_{16}H_{18}ClN_3S$, λ_{max} 664 nm, ≥97.0%) were purchased from Merck (Germany) and Sigma-Aldrich (Germany), respectively, and used as received. Fresh leaves of *Ophiorrhiza mungos* (*Om*) were collected from the forest/hilly areas of Chittagong University, Bangladesh. Deionized (DI) water (resistivity of 18 MΩ cm) and analytical grade reagents were utilized throughout. In our experiment, the glassware used were washed with distilled water and dried before use.

Preparation of Leaf Extracts. The plant leaves of *Om* were washed carefully with tap water and double-distilled water, followed by sun drying. Having the fresh leaves dried, they were powdered and stored. Then, 1 g of dried leaf powder was added to 100 mL of DI water with stirring at 80 °C for 30 min. After cooling, it was filtered utilizing Whatman No. 1, and the supernatant filtrate was collected for further use. The extract was used to prepare AgNPs without further treatment.

Synthesis and Characterization of *Om*-AgNPs. To synthesize *Om*-AgNPs, we followed the synthesis pathway that was described in detail in our recently published reports.[14] Briefly, 20 mL of prepared plant extracts was added dropwise (for 20 min) to 100 mL of $AgNO_3$ (aq.) solution (1 mM). The

https://doi.org/10.1021/acsomega.3c05992
ACS Omega 2024, 9, 4324−4338

Table 1. Different Adsorption Isotherm Models and Their Equations

adsorption isotherms	eqs		remarks	ref
Langmuir isotherm	$\frac{C_e}{q_e} = \frac{1}{K_L q_{max}} + \frac{C_e}{q_{max}}$	(3)	C_e = equilibrium concentration of MB dye (mg/L) q_e = quantity of MB dye adsorbed onto the AgNPs at equilibrium (mg/g) q_{max} = maximum monolayer adsorption capacity of adsorbent (mg/g)	32
	$R_L = \frac{1}{1 + K_b C_e}$	(4)	K_L = Langmuir adsorption constant (L/mg) K_b, R_L = constant	
Freundlich isotherm	$\log q_e = \log K_f + \frac{1}{n}\log C_e$	(5)	K_f = maximum adsorption capacity (mg/g) (mg/L)$^{1/n}$ n ($0 < n < 1$) = adsorption intensity or surface heterogeneity	
Temkin isotherm	$q_e = B \ln A + B \ln C_e$	(6)	b = Temkin constant A = Temkin isotherm constant (L/mg)	
	$B = \frac{RT}{b}$	(7)	B = constant related to heat of absorption (J/mol) T = absolute temperature (K) R = gas constant (8.314 J/mol K)	
Dubinin−Radushkevich Isotherm	$\ln q_e = \ln q_0 - \beta\varepsilon^2$	(8)	E = energy (kJ/mol)	
	$\varepsilon = RT\ln\left(1 + \frac{1}{C_e}\right)$	(9)	ε = adsorption potential	
	$E = \sqrt{1}/2\beta$	(10)	β = D−R isotherm constant (mol^2/kJ^2)	

mixture was stirred for 60 min at 80 °C. The dilute colloidal solution was kept still for 24 h for complete bioreduction at room temperature,[31] following centrifugation at 5000 rpm for 20 min. After washing, the prepared *Om*-AgNPs were subjected to drying overnight at 60 °C and stored at room temperature. To characterize *Om*-AgNPs, UV−visible (UV−vis) spectrophotometry, X-ray diffraction (XRD), Fourier transform infrared (FTIR) spectrophotometry, scanning electron microscopy (SEM), transmission electron microscopy (TEM), and energy-dispersive X-ray (EDX) analysis were applied, and their detailed methodologies were described in our recent published article.[14] X-ray photoelectron spectroscopy (XPS) measurements were performed on a Thermo Fisher Scientific XPS spectrometer (7×10^{-7} mbar pressure) equipped with an Al kα anode (1486.68 eV). The nanoparticles were mixed with ethanol and then dropped onto 1 × 1 cm cut slide glass, where they were then analyzed in a spectrometer. High-resolution spectra (narrow scans) were recorded for the Si 2p, Ca 2p, Ag 3d, C 1s, O 1s, and N 1s regions. Data were examined using the Avantage1 software, and it is noted that curve fitting and deconvoluted data were obtained from the software. Brunauer−Emmett−Teller (BET) surface areas were determined on a Micromerities ASAP 2000 surface analyzer at 77 K.

Adsorption Studies. The adsorption behavior of *Om*-AgNPs was studied through a batch process in heterogeneous catalysis. To investigate the catalytic performance of *Om*-AgNPs, first, MB dye solution was prepared by dissolving 0.0010 g of it in 100 mL of DI water and keeping it in the dark at room temperature. Afterward, the effects of MB concentration (10−50 mg/L), contact time (5−60 min), *Om*-AgNPs concentration (20−800 mg/L), and temperature (298−318 K) on the dye adsorption were investigated in batch experiments (pH = 7.4). The adsorption experiments were performed in a 50 mL beaker containing 25 mL of the MB solution and an appropriate amount of *Om*-AgNPs in the dark under continuous stirring (250 rpm) for a definite time period at predefined conditions. The mixture was heated to the desired temperature and stirred at 250 rpm. The solution was then filtered, and the concentration of unadsorbed dye was analyzed using a UV−vis device (UV-1800, Shimadzu, Japan) at 664 nm by collecting the samples at regular time intervals. Moreover, the degradation of MB with *Om* leaf powder and the aqueous extract of Om leaf was also investigated under the optimum conditions, as determined during the adsorption course with *Om*-AgNPs. To evaluate the reusability of the catalyst, the successive catalytic activities of *Om*-AgNPs were explored following the protocol reported by Asmare et al. with slight modifications.[22] For the first cycle, 15 mg of *Om*-AgNPs was added into the mixture of 25 mL of MB (10 mg/L) aqueous solution. The mixture was stirred for predefined times at 250 rpm, and the *Om*-AgNPs were collected through 20 min centrifugation at 4000 rpm and then washed with DI water and reused for additional five cycles under the same reaction conditions as described above. The percent (%) adsorption of MB and the quantity adsorbed at the given time t were calculated as follows (eqs 1 and 2)

$$\%\ \text{Removal} = \frac{C_i - C_f}{C_i} \times 100 \quad (1)$$

$$q_t = \frac{(C_i - C_t)V}{M} \quad (2)$$

where, q_t is the amount of MB adsorbed per unit mass of the adsorbent (mg/g), C_i is the initial MB concentration (mg/L), C_f is the final MB concentration (mg/L), C_t is the residual concentration at time t, V is the volume of MB solution (mL), and M is the mass of the adsorbent (g). Experiments were performed in triplicate, and the results were reported as mean ± SD.

Adsorption Isotherms. The four popular and significant isotherms (Table 1), Langmuir (eqs 3 and 4), Freundlich (eq 5), Temkin (eqs 6 and 7), and Dubinin−Radushkevich (D−R) (eqs 8−10) were used in the current work to examine the adsorption of MB onto *Om*-AgNPs. According to Langmuir, adsorption occurs uniformly or homogeneously within and/or on to the adsorbent (*Om*-AgNPs) surface.[32] The Freundlich isotherm illustrates the heterogeneity of adsorption sites, however, with an opposite (nonuniform) energy-level distribution.[32] The Temkin isotherm shows the effects of indirect adsorbate/adsorbent interaction on the adsorption isotherms, and the interactions involved with the heat of adsorption were also explained by Temkin.[32] The relationship between the energy of adsorption and the physisorption and/or chemisorption involved is explained by the D−R model.[32]

https://doi.org/10.1021/acsomega.3c05992
ACS Omega 2024, 9, 4324−4338

Table 2. Different Adsorption Kinetic Models with Their Equations

adsorption kinetics	eqs		remarks	ref
pseudo-first-order	$\ln (q_e - q_t) = \ln q_e - k_1 t$	(11)	q_e = quantity adsorbed at equilibrium (mg/g) q_t = quantity adsorbed at time t (mg/g) k_1 = rate constant (min^{-1})	32
pseudo-second-order	$\frac{t}{q_e} = \frac{1}{k_2 q_e^2} + \frac{1}{q_e}$	(12)	k_2 = rate constant (g/mg min)	
Elovich kinetic model	$q_t = \frac{1}{\beta}\ln(\alpha\beta) + \frac{1}{\beta}\ln t$	(13)	α = initial adsorption rate constant β = surface coverage constant	
intraparticular diffusion kinetic equations	$q_t = k_p \sqrt{t} + C$	(14)	k_p = intraparticular diffusion rate constant (mg/(g $min^{1/2}$)) C = intercept indicating thickness of the boundary layer (mg/g)	

Adsorption Kinetics. The kinetics phenomenon was evaluated by fitting the experimental values to pseudo-first order (PFO) (eq 11), pseudo- second-order (PSO) (eq 12), Elovich kinetic model (eq 13), and intraparticular diffusion (IPD) kinetic (eq 14) eqs (Table 2). Adsorption kinetics is commonly detected to be a function of adsorbate concentration.

Notably, the amount of dye absorbed from the liquid phase determines how quickly MB dye adheres on to the surface of the biosynthesized *Om*-AgNPs adsorbent in PFO and PSO kinetic models.[30] Besides, the Elovich model describes the adsorption process as chemisorption, whereas IPD model is necessary to know the rate-limiting step in the adsorption process.[32]

Adsorption kinetics were certified with the nonlinear Chi-square test (eq 15), correlation coefficient, and root-mean-square error (RMSE):

$$\chi^2 = \sum_{i=1}^{n} \frac{(q_{exp} - q_{cal})^2}{q_{cal}} \quad (15)$$

The Boyd model is provided by eqs 16 and 17 in order to predict the actual slow step interlaying in the adsorption process.

$$F = \frac{q_t}{q_e} \quad (16)$$

$$B_t = -0.4977 - \ln(1 - F) \quad (17)$$

F represents the fraction of solute adsorbed at any time, t, and B_t is a mathematical function of F.

Adsorption Thermodynamics. Thermodynamic parameters are evaluated using the following equations (eqs 18−20):

$$\ln K^\circ = \frac{\triangle S^\circ}{R} - \frac{\triangle H^\circ}{RT} \quad (18)$$

K_o is calculated from q_e/C_e, T is the temperature (K), and R is the gas constant. ΔS^0 is the change in entropy, and ΔH^0 is the change in enthalpy which can be obtained from the plot of ln K_o against $1/T$.

$$\triangle G^\circ = -RT\ln K^\circ \quad (19)$$

ΔG^0 is the change in free energy.

$$\ln k_2 = -\frac{E_a}{RT} + \ln A \quad (20)$$

k_2 is the rate constant, E_a is the activation energy, and A is the Arrhenius constant.

RESULTS AND DISCUSSION

Characterization of the Synthesized AgNPs. The material (*Om*-AgNPs) was prepared using the aqueous leaf extract of *Om* and $AgNO_3$ (1 mM) at 80 °C.[14] Figure 1a shows

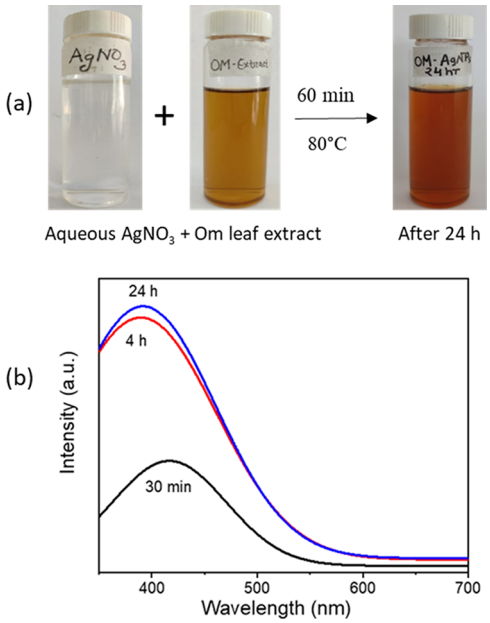

Figure 1. (a) Color change and (b) UV−visible spectra during the formation of *Om*-AgNPs (photographs courtesy of S. Ganguli et al. Copyright 2023).

the color change of the aqueous *Om* extract from yellow to deep-brown during the synthesis due to the surface plasmon resonance (SPR) characteristic of AgNPs.[14] The material was intensely characterized by UV−vis, XRD, SEM, TEM, EDX, FTIR, XPS, and N_2 gas adsorption−desorption analyses. A sharp and single absorbance peak at 413 nm (Figure 1b) was observed by UV−vis analysis, revealing the successful synthesis of *Om*-AgNPs. It is worthwhile to mention that the successive color change of the solution over the course of 24 h similar to the UV−vis spectra can be observed from our recent report as well.[14]

The XRD patterns of *Om*-AgNPs are shown in Figure 2a. The diffraction peaks are assigned to the (210), (122), (111), (200), (231), (142), (241), (220), and (311) silver crystalline planes of the face-centered cubic structure (JCPDS, file No. 04-0783).[14] The SEM and TEM images at different magnifications are shown in Figures 2b,d and 3a−c. Agglomerates with spherical morphology with variable sizes were observed in the SEM images (Figure 2b−d). A spherical

https://doi.org/10.1021/acsomega.3c05992
ACS Omega 2024, 9, 4324−4338

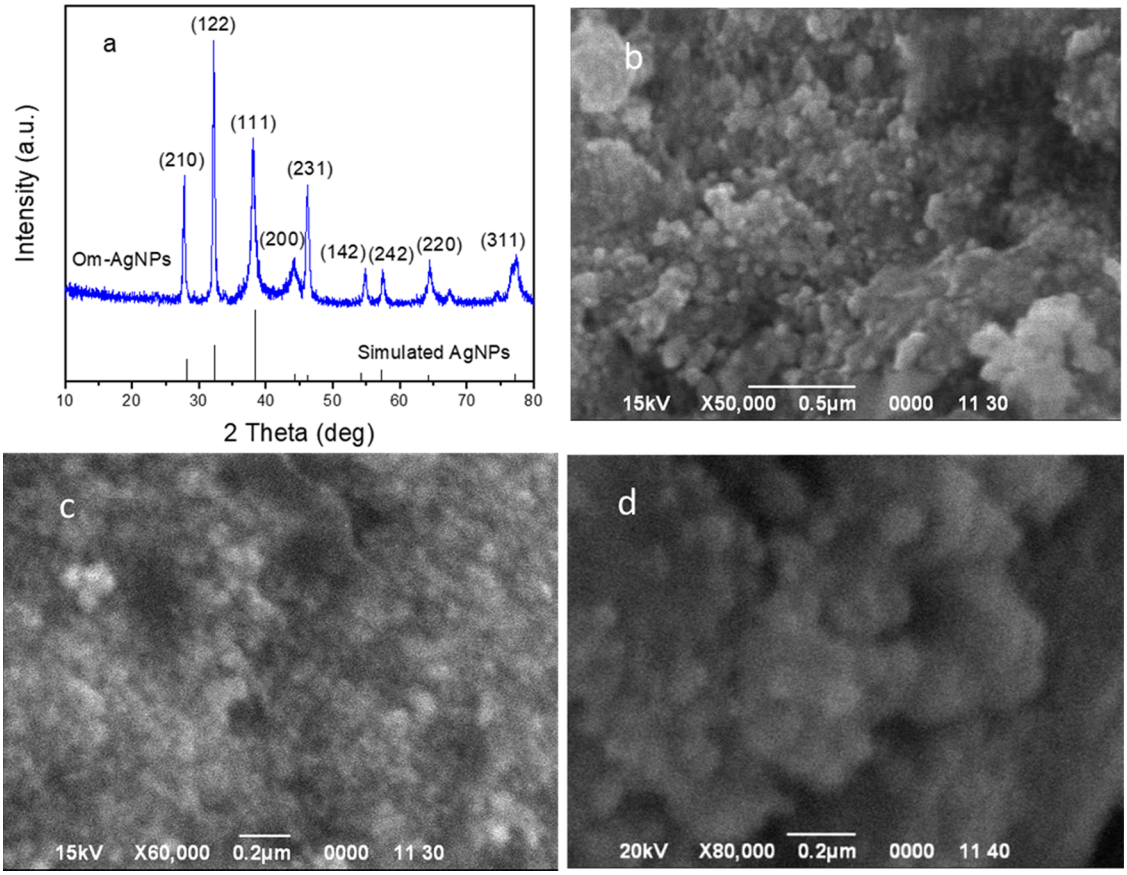

Figure 2. (a) XRD patterns and (b–d) SEM images at different magnifications of fresh *Om*-AgNPs.

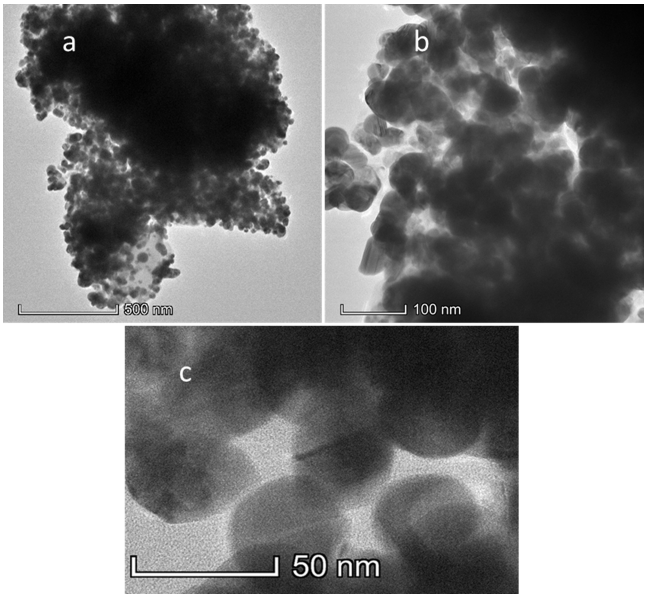

Figure 3. TEM images of fresh *Om*-AgNPs at different magnifications of (a) 500, (b) 100, and (c) 50 nm.

size of ca. 17 nm was confirmed by the TEM images (Figure 3a–c). EDX data exhibited a strong signal at 3 keV due to AgNPs as silver elements (Figure 4a).[14] The weight percentage of silver, oxygen, and carbon are 64.91, 22.46, and 12.63%, respectively.

The FTIR spectra of both *Om* and *Om*-AgNPs show identical characteristic peaks (Figure 4b,c). The bands

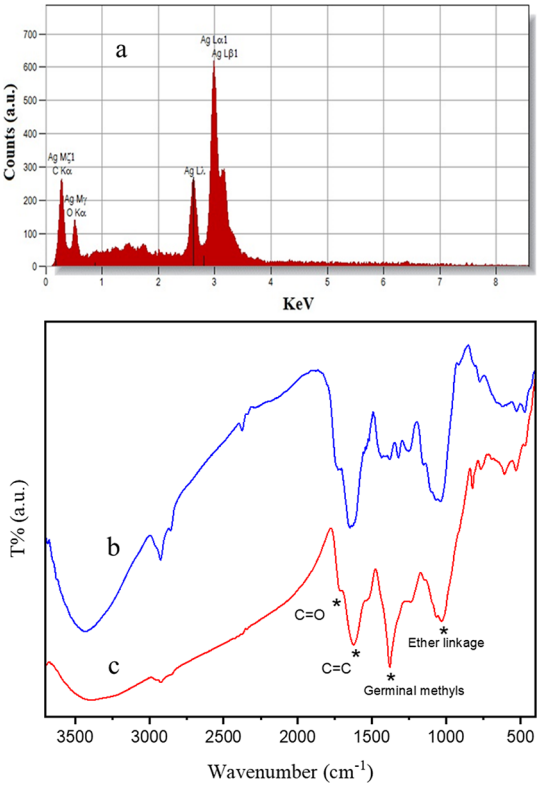

Figure 4. (a) EDX spectra of *Om*-AgNPs and FTIR spectra of (b) leaf extract and (c) *Om*-AgNPs.

https://doi.org/10.1021/acsomega.3c05992
ACS Omega 2024, 9, 4324–4338

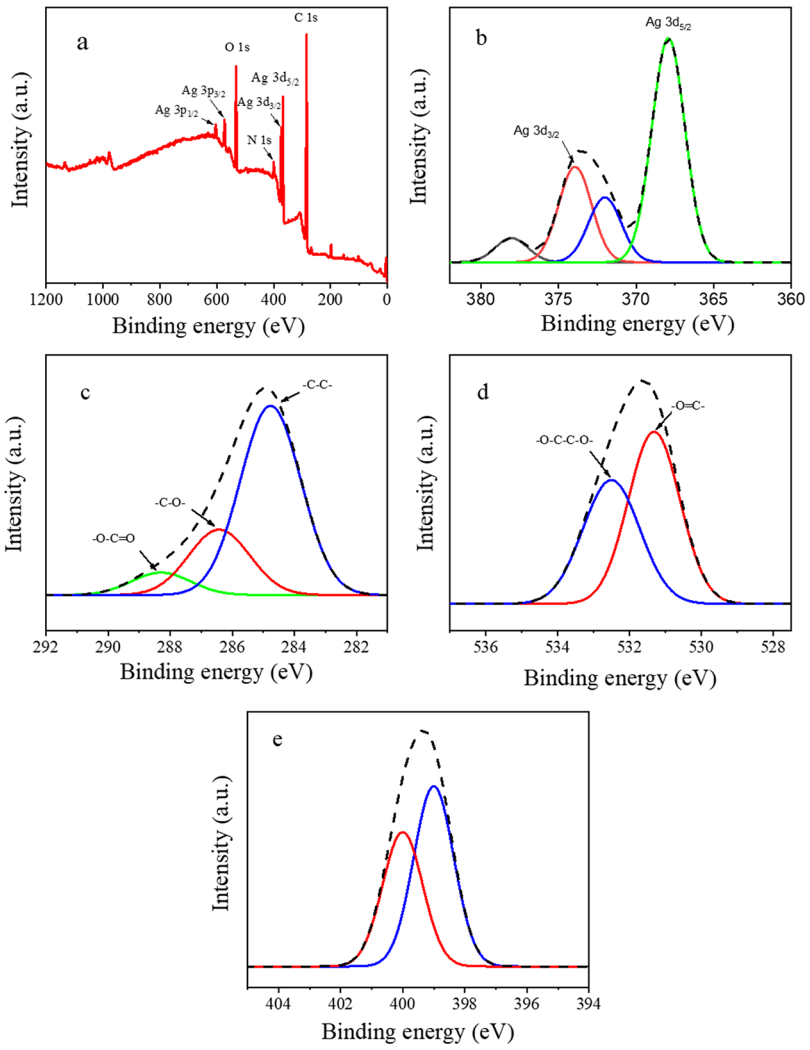

Figure 5. XPS spectra of *Om*-AgNPs of (a) survey, (b) Ag 3d, (c) C 1s, (d) O 1s, and (e) N 1s.

appearing at 1725, 1620, 1535, 1380, and 1065 cm^{-1} are assignable to the carbonyl group, C═C aromatic rings, C═C alkene, germinal methyl group, and ether linkages, respectively, confirming that AgNPs surfaces may contain biomolecules, which assisted in the formation of AgNPs and afterward stabilization.[20] The chemical composition and oxidation state of the biosynthesized AgNPs were confirmed by X-ray photoelectron spectroscopy. The survey spectrum (Figure 5a) exhibited four strong peaks at ∼370, ∼285, ∼531, and ∼400 eV due to silver [Ag 3d], carbon [C 1s], oxygen [O 1s], and nitrogen [N 1s], respectively, indicating the presence of Ag metal and biomolecules of leaf extract capped to AgNPs.[33,34]

The Ag 3d high-resolution spectrum in Figure 5b shows two peaks at the electron binding energy values of 367.91 and 373.95 eV owing to the spin−orbit splitting of Ag $3d_{5/2}$ and Ag $3d_{3/2}$ core levels, respectively.[34] In addition, the XPS spectrum shows peaks at 372.08 and 378.03 eV due to the presence of oxidized species of silver, viz., AgO or AgO_2.[35] The C 1s spectrum (Figure 5c) exhibits three peaks at 284.74, 286.38, and 288.24 eV, assigned to carbon −C−C−, −C−O−, and carboxyl carbon −O−C═O, respectively.[34,36] The O 1s spectra in Figure 5d display two peaks at the electron binding energy values of 531.31 and 532.50 eV. The former peak may be ascribed to oxygen in the − C═O group which is due to the bonding of oxygen to the surface of AgNPs, and the latter corresponds to the −O−C−C−O− bonds.[33,34] The XPS N 1s spectrum (Figure 5e) shows two peaks at 400.00 and 398.98 eV, indicating the strong interaction between organic amine or amide species and AgNPs.[33,37] Nevertheless, the presence of biomolecules such as flavonoids, alkaloids, and tannin on the surface of *Om*-AgNPs was identified by FTIR analysis and confirmed by XPS analysis.

Further, the surface properties of AgNPs can be obtained from the BET surface area analysis. The synthesized AgNPs showed typical N_2 adsorption isotherms (Figure 6). The N_2 adsorption and desorption isotherms are totally superposed, indicating that adsorption usually takes place in the micropores.[38] A capillary condensation step appears at the relative high-pressure region (P/P_o > 0.70) due to the capillary agglomeration phenomenon, and the isotherms rise very quickly and generate a lag loop. The specific surface area and pore volume were 4.39 m^2/g and 0.0129 cm^3/g, respectively.

Adsorption Study. The biosynthesized *Om*-AgNPs were evaluated for the removal of MB dye from water in the dark by varying the various reaction parameters.

Effect of Time, Adsorbate, and Adsorbent Concentration. The adsorbent dosage and time are the important factors in determining adsorption capacity because they define the reactive surface areas that are accessible for dye adsorption

https://doi.org/10.1021/acsomega.3c05992
ACS Omega 2024, 9, 4324−4338

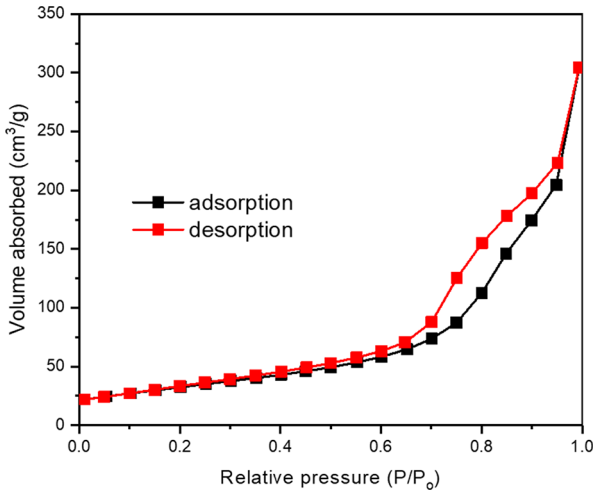

Figure 6. N_2 adsorption and desorption isotherms of *Om*-AgNPs (adsorption and desorption).

on the adsorbent.[39] Here, the effect of time and *Om*-AgNPs concentration (20−800 mg/L) on MB dye adsorption was examined in 20 mL of dye solutions (10 mg/L) at 25 °C. As can be seen from Figure 7a, the percent of adsorption increases with time from 34.4 ± 0.80% to 88.1% ± 1.74% as the dosage of the adsorbent increases from 20 to 800 mg/mL. For the initial 10 min, the adsorption rate (%) was very fast due to the availability of the binding site; then, it starts to adsorb slowly and reached the maximum within 60 min. However, the dye molecules are incompetent in reaching the available binding site when the adsorbent dose is higher (800 mg/L), thereby decreasing the rate of adsorption[39] and producing a clouding effect after the initial time period and attaining equilibrium in 60 min. After equilibrium was established, there was no visible change in the rate of adsorption, demonstrating that all of the *Om*-AgNPs adsorption sites were fully filled with dye molecules.[40] Afterward, adsorbent doses of 600 mg/L and 60 min time were selected for further experiments to achieve significant results. To evaluate the impacts of the initial dye concentration, an experiment has been performed, considering a dose of 600 mg/L, contact time of 60 min, and concentration of 10−50 mg/L at 25 °C (Figure 7b). Initially, the number of dye moles is higher than that of the *Om*-AgNPs surface area. Therefore, the adsorption capacity of *Om*-AgNPs increased from 16.51 to 59.35 mg/g with an increasing concentration of MB dye. The ideal dye concentration for additional adsorption studies was therefore determined to be 10 mg/L. The adsorption capacity increases with the dye concentration because at low concentrations there could be some unoccupied active sites on the surface of *Om*-AgNPs. In addition, the driving force for the mass transfer also could increase with the increase in dye concentration. A similar phenomenon was also observed elsewhere.[28]

It has to be noted that at the optimum dosage and equilibrium condition (600 mg/L of *Om*-AgNPs, 10 mg/mL of MB dye, and 60 min), the *Om* leaf powder and water extract of *Om* showed removal efficiencies of 57.34 ± 1.71 and 38.25 ± 0.91%, respectively (Figure 8a,b). The lower adsorptive removal of MB dyes using the water extract of leaf powder as compared to raw leaf powder presumably suggests the possible variation in the phytochemical content of leaf powder and in their water extract. Hence, it is also indicated that our synthesized *Om*-AgNPs possessed a better adsorptive removal capacity than *Om* leaf and their water extract. Moreover, it was interesting that during the course of adsorptive removal of MB dyes using the leaf powder and water extract of *Om* leaf, the pH of the aqueous solution remained 7.4 throughout the process, while in the case of using *Om*-AgNPs, the pH was shifted from 7.4 to 8.0. Previous work demonstrated that the features of AgNPs also vary with the pH value during synthesis.[41] Therefore, the present results indicated that changing the pH value from 7.4 to 8.0 might also provide some additional surface properties of *Om*-AgNPs and subsequently better capacity to remove dyes.

Adsorption Isotherms. Langmuir, Freundlich, Temkin, and D-R isothermal models were adopted to examine explicitly the relationship between the adsorbed amount of MB dye and its content.[32] Figure 9a−d and Table 3 display the Langmuir, Freundlich, Temkin, and D-R isotherm plots and the parameters derived from them. The correlation coefficient (R^2) and RMSE values were utilized to identify the best-fit model which describes the adsorption process. The closer R^2 is to unity (1.0) and lower the RMSE value, the greater is the concordance between the experimental data and the model's predicted value and the best fit. Comparing R^2 and RMSE value isotherms, Langmuir (0.9956 and 0.0062), Freundlich

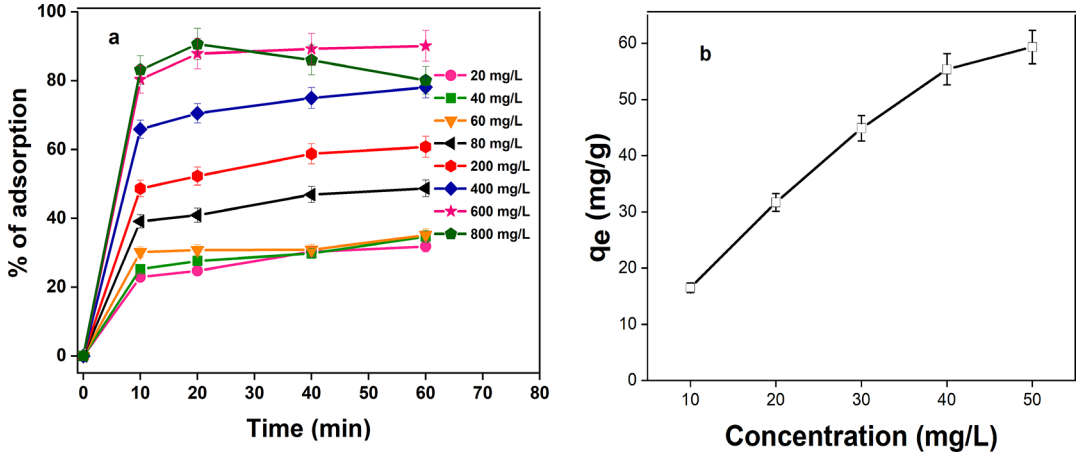

Figure 7. (a) Effect of time and *Om*-AgNPs concentration on the adsorption of MB dye molecules and (b) effect of dye concentration on *Om*-AgNPs.

https://doi.org/10.1021/acsomega.3c05992
ACS Omega 2024, 9, 4324−4338

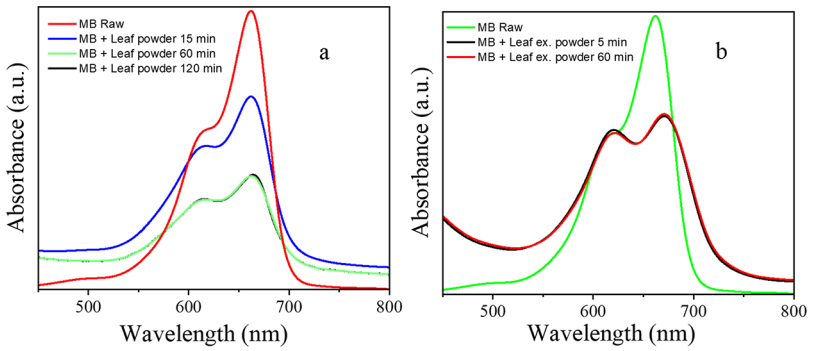

Figure 8. UV−visible spectra of MB dye removal efficiency using (a) leaf powder and (b) leaf extract powder at different time intervals.

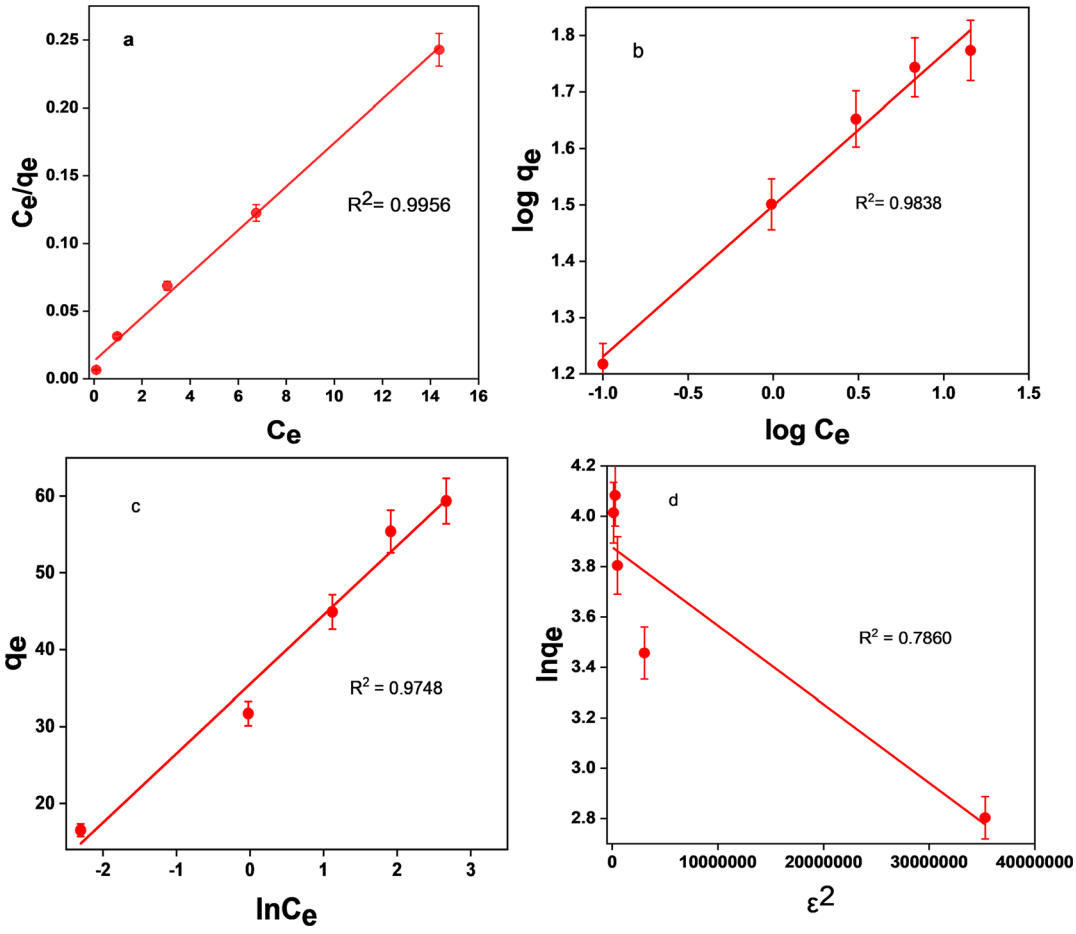

Figure 9. (a) Langmuir, (b) Freundlich, (c) Temkin, and (d) D−R adsorption isothermal plots for the adsorption of MB dye onto *Om*-AgNPs.

(0.9838 and 0.0289), Temkin (0.9748 and 2.7991), and D-R (0.7860 and 0.2423) values (Table 3) indicate that the Langmuir isotherm (Figure 9a) best-fits the adsorption of MB dye on *Om*-AgNPs, indicating a monolayer and homogeneous adsorption process with all adsorption sites, holding equal affinity for the adsorbate.[42] If the value of R_L (Langmuir constant) falls within the range $0 < R_L < 1$, the adsorption process is deemed advantageous. As determined by the results of this study (Table 3), R_L is 0.041, indicating that the adsorption phenomenon was fruitful.[43] The maximum adsorption (q_{max}) capacity found from the Langmuir plot is 80.451 mg/g, which was compared to that of others reported earlier[19−21,29,30,32,39,44−52] (Tables 4 and 5). The best fittings of the Langmuir model typically describe the chemisorption process that has been taken place at the surface.[29,53] The observed Langmuir adsorption constant (K_L) value indicates that adsorption is spontaneous in nature.[39] Moreover, it is very interesting to observe that the R^2 value from the Freundlich (0.9838) and Temkin (0.9748) plots were also close to 1, whereas the RMSE value of the Temkin model (2.7991) is high, indicating that the Freundlich model (Figure 9b) also explained the adsorption behavior. The R^2 value is sufficiently close (>0.98) to 1, and the low value of RMSE from the Freundlich model also indicates that physisorption might have also taken place at the surface.[53] In addition, the value of adsorption intensity (n), typically from 1 to 10, is indicated as the favorable condition for adsorption, and the high value of n in our case (n = 3.726) is indicated as the favorable adsorptive

https://doi.org/10.1021/acsomega.3c05992
ACS Omega 2024, 9, 4324−4338

Table 3. Comparison of the Coefficient Isotherm Parameters for MB Dye Adsorption onto *Om*-AgNPs

isotherms	constants	value
Langmuir	q_{max} (mg/g)	80.451
	K_L (L/mg)	0.772
	R_L	0.041
	R^2	0.9956
	RMSE	0.0062
Freundlich	N	3.726
	K_f	31.547
	R^2	0.9838
	RMSE	0.0289
Temkin	B (J/mol)	9.007
	A (L/g)	51.483
	B	275.087
	R^2	0.9748
	RMSE	2.7991
Dubinin−Radushkevich	q_o (mg/g)	48.282
	β (mol^2/kJ^2)	0.000000031
	E_a (kJ/mol)	4004.564
	R^2	0.7860
	RMSE	0.2423

condition and *Om*-AgNPs as a better adsorbent.[39,54] Even though the Temkin model (Figure 9c) is not best suited in our case, the high and positive value of the Temkin constant (A and b) represents a good binding affinity between *Om*-AgNPs and MB and the endothermic adsorption process.[55] Interestingly, the Temkin constant related to the heat of sorption (B) value (9.007 J/mol) concluded that adsorption is governed by both physisorption and chemisorption.[55] The R^2 value of the D−R model (Figure 9d) is far behind 1 (0.7860); nevertheless, the important adsorption energy (E) parameter value is very high (4004.564 kJ/mol), which is possibly due to chemisorption.[56,57] Therefore, considering the above findings, it can be anticipated that chemisorption and physisorption originated and played the key role, indicating cooperative multilayer adsorption. In the literature, there are abundant reports explaining the adsorption nature of physisorption or chemisorption based on the different isotherm models; however, cooperative multilayer adsorption was rarely reported.[55,58] The present findings should be cautiously handled to commercialize our adsorbent as the isotherm model has few limitations even though it is used by many researchers.[29,32,39,40,44,50] On one hand, after observing much literature, only a few reports have been found based on the green-synthesized AgNPs-mediated adsorptive removal of MB dye, presumably suggesting poor understanding on this subject. Table 4 represents a comparison of q_{max}, kinetics, and catalyst dose of different green-synthesized AgNPs and AgNPs-loaded nanocomposites that has been previously reported. It represents that *Om*-AgNPs are relatively efficient adsorbents as compared to previously reported green-synthesized AgNPs[20,29,30,32] and nanocomposites as adsorbents.[19−21,39,50] On the other hand, considerably many reports have been found based on the adsorptive removal of textile dyes using plant-based waste. Table 5 represents the q_{max} values of MB dye with the other plant-based waste adsorbents. Even by comparing to these, our synthesized *Om*-AgNPs showed a good maximum monolayer adsorption capacity even at a lower catalyst dose.[44−49,51,52] For instance, mango peels,[59] rubber leaf,[60] banana peels,[61] and corn cob[62] showed better adsorptive capacity than *Om*-AgNPs, nevertheless their catalyst doses were much higher than ours'. It is worthwhile to mention that few bioadsorbents showed better performance and few performed low (Tables 4 and 5). It is probably due to the variation in the presence of phytochemicals in the bioadsorbent and on the AgNPs surface. Moreover, the size, shape, and other confounding factors could not be ruled out at this moment.

Table 5. Comparison of q_{max} (mg/g) Values with Other Bioadsorbents

adsorbent	adsorbent dose (mg/L)	temp. (K)	q_{max} (mg/g)	kinetic model	ref
mango peels	1400	303	277.8	PSO	59
rubber leaf	1000	303	263.2	PSO	60
banana peels	800	303	250	PFO	61
corn cob	1200	303	216.6	PFO	62
***Om*-AgNPs**	**600**	**298**	**80.451**	**PSO**	**this study**
coconut shell	1000	303	50.6	PSO	51
bagasse	4000	300−333	49.8−56.5	PSO	52
Ficus carica	5000	298−323	47.62	PSO	44
Parthenium hysterophorus	4000	298	39.7		45
Delonix regia pods	2000	298	23.3		46
wild carrot	500	298	21	PSO	47
lantana camara stem	500−2000	298	19.84	PSO	49
sunflower oil cake	2000	288−318	16.43	PSO	48

Table 4. Comparison of q_{max} (mg/g) Values of Various AgNPs and/or Nanocomposites for Dye Adsorption

green-synthesized	catalyst (dose, mg/L)	temp. (K)	model dye	q_{max} (mg/g)	kinetic model	ref
AgNPs	40	room	MB	218.95	PFO	29
AgNPs	2000	room	MB	121.04	PSO	30
***Om*-AgNPs**	**600**	**298−318**	**MB**	**80.451**	**PSO**	**this study**
AgNPs	200−1000	303	rhodamine B (RhB)	59.85	PSO	32
AgNPs	5	room	MB	49.26		20
Nanocomposites						
AgNPs/GG/Poly(AA)	600	298−318	MB	833.33	PSO	21
AlG@AgNPs	10	303	crystal violet	186.93	PSO	39
AgNPs/GO (1−100 mM)		room	MB	137.50−365.00	PSO	19
green-synthesized *Om*-AgNPs	**600**	**298−318**	**MB**	**80.451**	**PSO**	**this study**
AgCS composite	100	303−308	MB	50.51		20
STpe-AgNP	0.06	room	BB (bromophenol blue)	9.6	PSO	50

https://doi.org/10.1021/acsomega.3c05992
ACS Omega 2024, 9, 4324−4338

Adsorption Kinetics. As part of the kinetics study, the rate of MB dye elimination and its regulating mechanism were investigated. The parameter values of different kinetic models such as PFO (Table 6 and Figure 10a), PSO (Table 6 and Figure 10b), Elovich (Table 6 and Figure 10c), and IPD (Table 6 and Figure 10d) were used to describe the MB dye uptake on to *Om*-AgNPs. Gowda et al.[29] and Azeez et al.[32] studied the abovementioned kinetic modes. The correlation coefficient (R^2) was used to measure how well experimental and computed data fit together. A nonlinear χ^2 test was also used to compare experimentally measured and estimated data. In addition, a lower RMSE value also indicates the best-suited model.[63]

Table 6. Different Kinetic Parameters for MB Dye Adsorption onto *Om*-AgNPs

q_e experimental (mg/g)	16.51
PFO	
q_e, calculated (mg/g)	10.23
k_1 (min^{-1})	−0.001
R^2	0.8323
χ^2	3.851
RMSE	0.8117
PSO	
q_e, calculated (mg/g)	16.67
k_2 (g/mg min)	0.023
R^2	0.9980
χ^2	0.002
RMSE	0.0612
Elovich	
α	131.18
B	0.504
R^2	0.9948
RMSE	0.1769
IPD	
k_p (mg/g $min^{-1/2}$)	1.013
C (mg/g)	9.17
R^2	0.9164
RMSE	0.7096

In a nut shell, an equilibrium kinetic model that successfully describes the data has a value of R^2 relatively close to unity, low χ^2, and RMSE value.[63] Comparison of R^2, χ^2, and RMSE values (Table 6) of PFO (R^2 = 0.8323, χ^2 = 3.851, RMSE = 0.8117) (Figure 10a), PSO (R^2 = 0.9980, χ^2 = 0.002, RMSE = 0.0612) (Figure 10b), and Elovich (R^2 = 0.9948, RMSE = 0.1769) (Figure 10c) kinetic models shows that the PSO kinetic model (Figure 10b) seems mostly applicable for explaining the process and rate of uptake of MB dye on to synthesized *Om*-AgNPs. The PSO kinetic model, for characterizing the adsorption rate, is similarly validated by a lower value of χ^2 and RMSE. It is noticeable that the calculated value of q_e (16.67 mg/g) also well matched with the experimental value (16.51 mg/g) obtained from the PSO model than that from the PFO model ($q_{e(cal)}$ = 10.23 mg/g and $q_{e(exp)}$ = 16.51 mg/g) (Table 6). This shows that the adsorption mechanism may involve chemisorption.[32] In addition, IPD is one of the many variables that influence the adsorption rate.[32] Figure 10d shows the results of research into the potential impact of IPD on the adsorption course. The Boyd model, as described in eqs 16 and 17, was utilized to further examine the rate-controlling stage in the adsorption course, and the results are represented in Figure 11.

IPD of *Om*-AgNPs-MB was plotted as a single linear process, however, not considered as the only rate-controlling step. The Boyd plot confirmed this, which showed that it did not pass through the origin. Therefore, it indicated that during the adsorption process, surface adsorption and intraparticle diffusion occurred concurrently.[64,65] The boundary layer thickness is indicated by the value of *C* (intercept), and the greater the value of C, the greater is the influence of the boundary layer diffusion.[64]

Thermodynamic Studies. Thermodynamic variables (ΔG^0, ΔH^0, and ΔS^0) determined from $\ln K_0$ against the 1/T plot for the adsorption of MB on *Om*-AgNPs are presented in Table 7 and Figure 12a. Activation energy (E_a) is calculated from the Arrhenius plot (Table 7 and Figure 12b). These variables provide details regarding the spontaneity of the process.[66] In the present study, the positive values of enthalpy indicate that the adsorption process is endothermic in nature, while the value of ΔH^0 equal to 4.91 kJ/mol depicted physisorption,[67] which is opposite to the finding from the PSO model that suggested chemisorption. In addition, the estimated ΔG^0 value was found to be between −11.10 and −12.18 kJ/mol, so it was possibly inferred that sorption was a physical spontaneous process.[67] The ΔG^0 value that remained between 0.0 and −20.0 kJ/mol indicated physisorption.[68] Moreover, the decreases in ΔG^0 value with increasing temperature might indicate reduction in spontaneity at a higher temperature.[67] The positive entropy (ΔS^0 = 53.69 J/mol K) designates the possible interactions of MB dye on to the surface of *Om*-AgNPs,[21] corresponding to the high degree of randomness.[21] The degree of activation energy (E_a) provides information regarding the physisorption or chemisorption nature of the adsorption course.[66] Based on the E_a value (43.1 kJ/mol) in the present investigation, the adsorption process is recognized as chemisorption because the E_a range for chemisorption is usually between 40 and 800 kJ/mol.[66] Thermodynamic parameters such as ΔH^0, ΔG^0, and ΔS^0 inferred the adsorption process as physisorption, whereas the E_a value sheds light toward chemisorption. Thus, the overall results obtained from isotherms, kinetics, and thermodynamic analyses possibly suggested that both physisorption and chemisorption were responsible for the adsorptive removal of MB dye from water.

Stability of Adsorbent. The stability of adsorbents is the most significant aspect for their industrial uses. The stability of the adsorbent was calculated with the degradation of MB in water by repeated reuse of the material in the same manner as described above. At the end of each run, the adsorbent was filtered off, washed with the solvent, dried, and reused. Figure 13 demonstrates that the material exhibited excellent stability across the fifth cycle of dye degradation. Only a 7.6 ± 1.33% drop in adsorption capacity was detected even after the fifth cycle. After the first cycle, the stability was assessed as about 88.1 ± 1.74% which fell to 80.5 ± 0.91% after the fifth cycle. The slight decrease in activity could be due to the saturating effect of intermediate products on the adsorptive sites. Overall, the activity of the synthesized adsorbent (*Om*-AgNPs) did not drop much. To examine the structural stability of the adsorbent, XRD analysis of the reused adsorbent was carried out. The XRD pattern and SEM image of the reused *Om*-AgNPs after the fifth cycle (Figure 14a,b) were identical to that of the fresh material (Figure 2a,d), suggesting that no structural change or agglomeration in the original framework

https://doi.org/10.1021/acsomega.3c05992
ACS Omega 2024, 9, 4324−4338

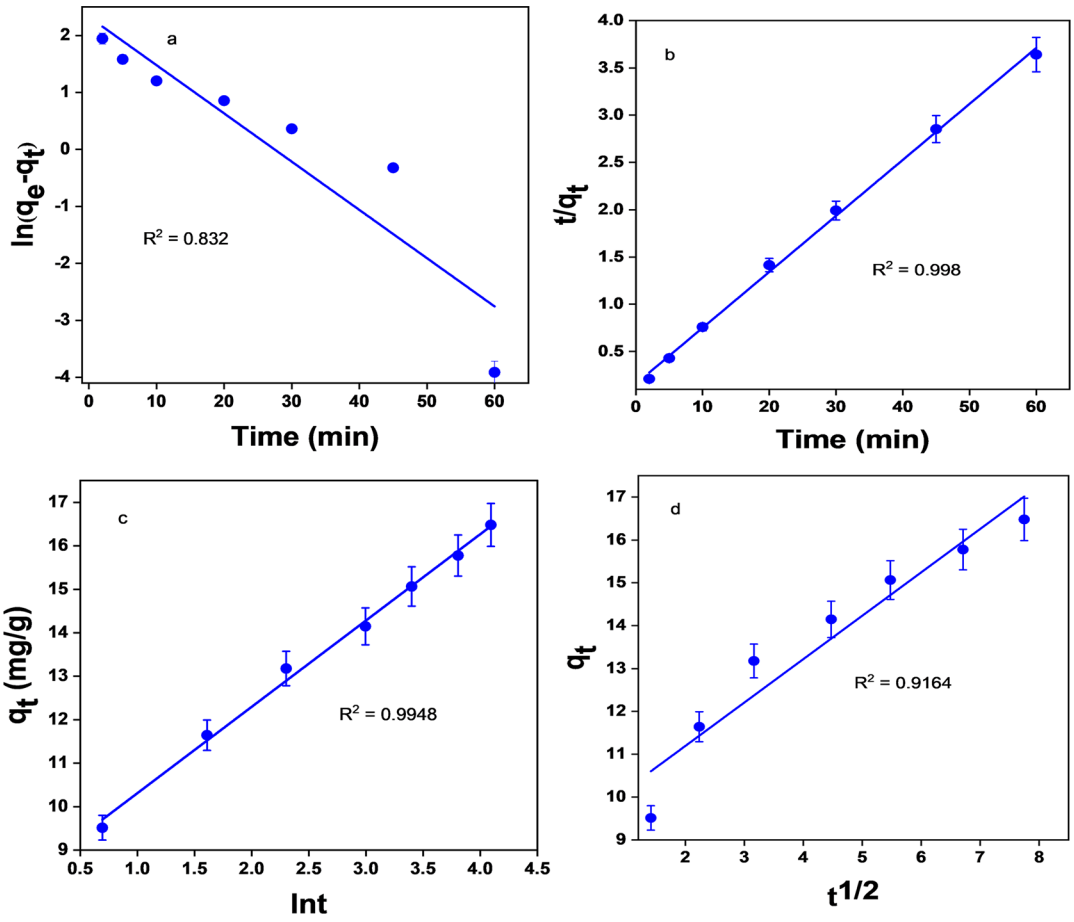

Figure 10. (a) PFO, (b) PSO, (c) Elovich, and (d) IPD models of the adsorption process of MB dye by *Om*-AgNPs.

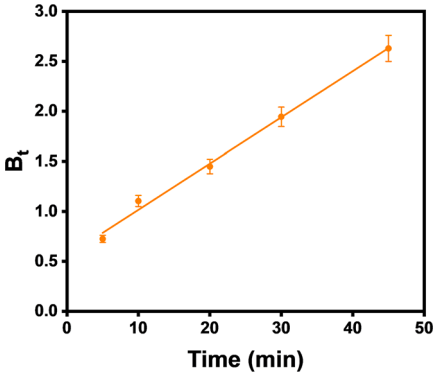

Figure 11. Boyd plot for the adsorption of MB onto *Om*-AgNPs.

Table 7. Thermodynamics for the Adsorption of MB Dye on to Synthesized *Om*-AgNPs

temperature (°C)	ΔH^0 (kJ/mol)	ΔG^0 (kJ/mol)	ΔS^0 (J/mol K)	E_a (kJ/mol)	R^2
25	4.91	−11.10	53.69	43.1	0.9871
35		−11.62			
45		−12.18			

of the AgNPs center took place during the adsorption processes. It is also interesting to note that the size of the *Om*-AgNPs calculated by the Debye−Scherrer (D−S) equation is comparable (17 and 16 nm for the fresh and reused catalyst, respectively), which also indicated that the structure of the AgNPs was retained after the recycle runs.

Mechanism. Based on the evidence from the reported data, the adsorption of MB dye onto *Om*-AgNPs through the *Om* biomolecules on the surface of AgNPs may occur through several cooperative interactions such as electrostatic interactions, $\pi-\pi$ stacking, and hydrogen bonds.[69] FTIR, XPS, and EDX analyses confirmed that *Om*-AgNPs contain several phytochemicals such as alkaloids, phenolic compounds, and flavonoids surrounding AgNPs, in which the C═O, C═C, or OH groups of the *Om*-AgNPs adsorbent surface can have affinity toward the cationic MB dye via electrostatic interactions.[70] Alternatively, the $\pi-\pi$ stacking mechanism may occur due to the presence of aromatic rings of both MB dye and biomolecules surrounding AgNPs. Kinetics results showed the presence of both chemical and physical adsorption processes on MB dye adsorption onto *Om*-AgNPs, further confirming the electrostatic interactions and $\pi-\pi$ stacking mechanism. In contrast, we also propose that in the present *Om* plant-mediated AgNPs-based MB dye removal system, the phytoconstituents, −OH, and −C═O groups present on the surface of the *Om*-AgNPs adsorbent[71] may interact with the cationic MB dye and get adsorbed onto the surface of *Om*-AgNPs via hydrogen bonding between the electronegative atoms (nitrogen and sulfur atoms) of MB dye and the hydroxyl groups of the adsorbent.[21] The AgNPs may be strengthened inside this composite matrix to enhance the surface energy of the *Om*-AgNPs adsorbent to afford greater binding of MB dye.

https://doi.org/10.1021/acsomega.3c05992
ACS Omega 2024, 9, 4324−4338

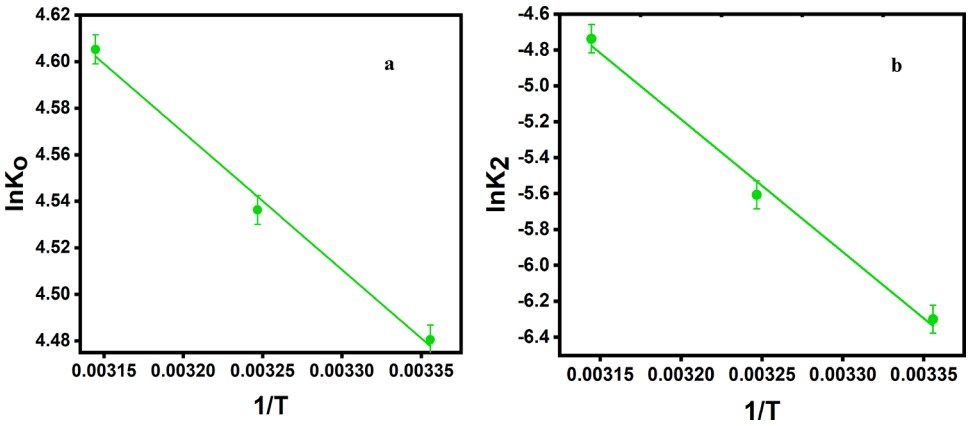

Figure 12. (a) Van't Hoff's plot for the adsorption of MB onto *Om*-AgNPs and (b) Arrhenius plot for the calculation of apparent activation energy

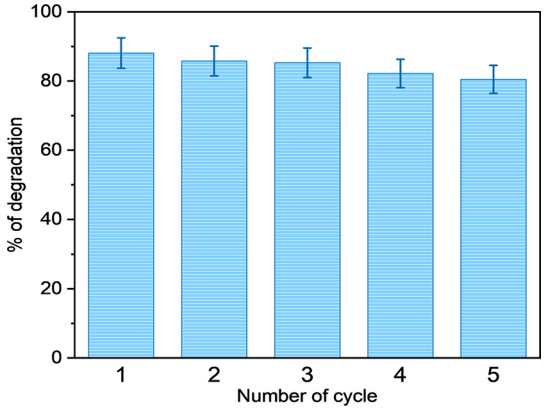

Figure 13. Recycle test of *Om*-AgNPs for MB dye removal.

CONCLUSIONS

The biosynthesis of AgNPs using an aqueous leaf extract of *Om*, *Om*-AgNPs, exhibited excellent catalytic efficiency in removing MB dye from water in the dark. The adsorption capacity was found to be dependent on the contact time, adsorbent dose, and concentration. The biosynthesis of AgNPs showed a better adsorptive removal capacity of MB dye from water (88.1 ± 1.74%) than the leaf extract (38.25 ± 0.91%) within a time period of 60 min at 298 K. The Langmuir isotherm model suitably fitted the best with the maximum monolayer capacity of 80.451 mg/g at 298 K, suggesting a chemisorption process. The Freundlich model was also considerably accepted, indicating the physisorption process in nature. The kinetic models for the adsorption process indicated that the adsorption of MB dye onto *Om*-AgNPs followed a pseudo-second-order reaction. The positive ΔG^0 and ΔH^0 values indicated an endothermic spontaneous process at the adsorbent−adsorbate surface, and physisorption was also governed in the process. The material could be reused five times without a significant loss of catalytic performance. The present biosynthesized AgNPs could be considered effective, reusable, and eco-friendly nanoadsorbents for the removal of the harmful dye MB from water without adding any external compounds for environmental restoration.

ASSOCIATED CONTENT

Supporting Information

The Supporting Information is available free of charge at https://pubs.acs.org/doi/10.1021/acsomega.3c05992.

List of phytochemicals found in the aqueous extract of *O. mungos* (PDF)

AUTHOR INFORMATION

Corresponding Authors

Benu Kumar Dey − *Department of Chemistry and Pro-Vice-Chancellor (Academic), University of Chittagong, Chattogram 4331, Bangladesh*; Email: benudey@yahoo.com

Samiran Bhattacharjee − *Centre for Advanced Research in Sciences (CARS), University of Dhaka, Dhaka 1000,*

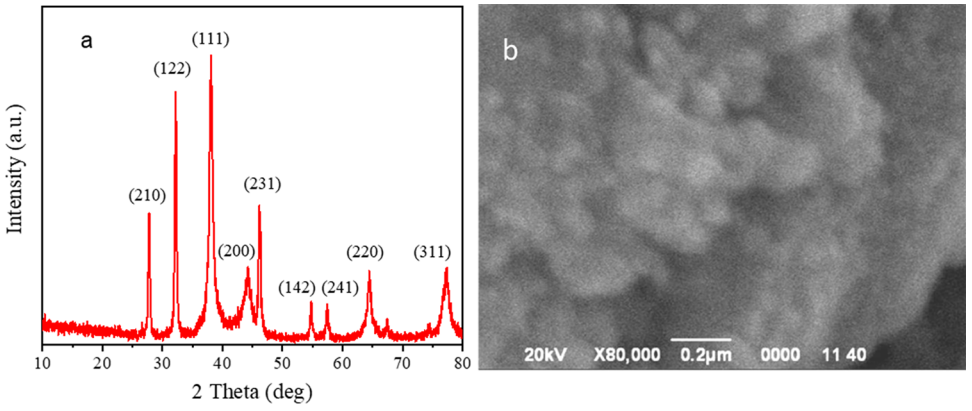

Figure 14. (a) XRD pattern and (b) SEM image of reused *Om*-AgNPs after the fifth cycle.

https://doi.org/10.1021/acsomega.3c05992
ACS Omega 2024, 9, 4324−4338

Bangladesh; orcid.org/0000-0002-9528-6552; Email: s.bhattacharjee@du.ac.bd

Sumon Ganguli − *Department of Applied Chemistry and Chemical Engineering and Biomaterials Research Laboratory (BRL), Department of Applied Chemistry and Chemical Engineering, University of Chittagong, Chattogram 4331, Bangladesh*; orcid.org/0000-0002-1944-7756; Email: sumonganguli@cu.ac.bd

Authors

Aklima A Akhi − *Department of Applied Chemistry and Chemical Engineering and Biomaterials Research Laboratory (BRL), Department of Applied Chemistry and Chemical Engineering, University of Chittagong, Chattogram 4331, Bangladesh*

Abid Hasan − *Department of Applied Chemistry and Chemical Engineering and Biomaterials Research Laboratory (BRL), Department of Applied Chemistry and Chemical Engineering, University of Chittagong, Chattogram 4331, Bangladesh*

Nakshi Saha − *Department of Applied Chemistry and Chemical Engineering and Biomaterials Research Laboratory (BRL), Department of Applied Chemistry and Chemical Engineering, University of Chittagong, Chattogram 4331, Bangladesh*

Sabbir Howlader − *Department of Applied Chemistry and Chemical Engineering and Biomaterials Research Laboratory (BRL), Department of Applied Chemistry and Chemical Engineering, University of Chittagong, Chattogram 4331, Bangladesh*

Sabonty Bhattacharjee − *Centre for Advanced Research in Sciences (CARS), University of Dhaka, Dhaka 1000, Bangladesh*

Kamol Dey − *Department of Applied Chemistry and Chemical Engineering, University of Chittagong, Chattogram 4331, Bangladesh*

A. K. M. Atique Ullah − *Nanoscience and Technology Research Laboratory, Atomic Energy Center, Bangladesh Atomic Energy Commission, Dhaka 1000, Bangladesh*; orcid.org/0000-0002-4545-2663

Farhana Rumzum Bhuiyan − *Laboratory of Biotechnology and Molecular Biology, Department of Botany, University of Chittagong, Chattogram 4331, Bangladesh*

Ashok Kumar Chakraborty − *Department of Applied Chemistry and Chemical Engineering, Islamic University, Kushtia 7003, Bangladesh*

Umme Sarmeen Akhtar − *Bangladesh Council of Scientific and Industrial Research (BCSIR), Dhaka 1205, Bangladesh*

Md. Aftab Ali Shaikh − *Bangladesh Council of Scientific and Industrial Research (BCSIR), Dhaka 1205, Bangladesh*

Complete contact information is available at: https://pubs.acs.org/10.1021/acsomega.3c05992

Notes

The authors declare no competing financial interest.

■ ACKNOWLEDGMENTS

The authors gratefully acknowledge the financial support by the BUGC postdoctoral fellowship program from the Bangladesh University Grants Commission (BUGC). They also acknowledge the support from Centre for Advanced Research in Sciences (University of Dhaka), Research and Publication Cell (University of Chittagong), Biomaterials Research Laboratory (Dept. of Applied Chemistry and Chemical Engineering, University of Chittagong), and Ministry of Education (Bangladesh). The authors gratefully acknowledge the experimental support from Bangladesh Council of Scientific and Industrial Research (BCSIR), Bangladesh, and Ms. Bithi Majumder, an Assistant Professor of English (Noakhali Science and Technology University, Bangladesh) for her assistance in grammar check.

■ REFERENCES

(1) Iravani, S. Green Synthesis of Metal Nanoparticles Using Plants. *Green Chem.* **2011**, *13* (10), 2638−2650.

(2) Twaij, B. M.; Hasan, M. N. Bioactive Secondary Metabolites from Plant Sources: Types, Synthesis, and Their Therapeutic Uses. *Int. J. Plant Biol.* **2022**, *13* (1), 4−14.

(3) Ghosh, S.; Patil, S.; Ahire, M.; Kitture, R.; Gurav, D. D.; Jabgunde, A. M.; Kale, S.; Pardesi, K.; Shinde, V.; Bellare, J.; Dhavale, D. D.; Chopade, B. A. Gnidia Glauca Flower Extract Mediated Synthesis of Gold Nanoparticles and Evaluation of Its Chemocatalytic Potential. *J. Nanobiotechnology* **2012**, *10*, 1−9.

(4) Bhosale, M. A.; Bhanage, B. M. Silver Nanoparticles: Synthesis, Characterization and Their Application as a Sustainable Catalyst for Organic Transformations. *Curr. Org. Chem.* **2015**, *19* (8), 708−727.

(5) Jiang, Z. J.; Liu, C. Y.; Sun, L. W. Catalytic Properties of Silver Nanoparticles Supported on Silica Spheres. *J. Phys. Chem. B* **2005**, *109* (5), 1730−1735.

(6) Ahmed, S.; Saifullah; Ahmad, M.; Swami, B. L.; Ikram, S. Green Synthesis of Silver Nanoparticles Using Azadirachta Indica Aqueous Leaf Extract. *J. Radiat. Res. Appl. Sci.* **2016**, *9* (1), 1−7.

(7) Ahmed, S.; Ahmad, M.; Swami, B. L.; Ikram, S. A Review on Plants Extract Mediated Synthesis of Silver Nanoparticles for Antimicrobial Applications: A Green Expertise. *J. Adv. Res.* **2016**, *7* (1), 17−28.

(8) Muthukrishnan, S.; Bhakya, S.; Muthukumar, M.; Sukumaran, M.; Rao, M. V.; Senthil Kumar, T. Catalytic Degradation of Organic Dyes Using Synthesized Silver Nanoparticles: A Green Approach. *J. Bioremed. Biodeg.* **2015**, *6*, 312.

(9) Ganapathy Selvam, G.; Sivakumar, K. Phycosynthesis of Silver Nanoparticles and Photocatalytic Degradation of Methyl Orange Dye Using Silver (Ag) Nanoparticles Synthesized from Hypnea Musciformis (Wulfen) J.V. Lamouroux. *Appl. Nanosci.* **2015**, *5* (5), 617−622.

(10) Saha, J.; Begum, A.; Mukherjee, A.; Kumar, S. A Novel Green Synthesis of Silver Nanoparticles and Their Catalytic Action in Reduction of Methylene Blue Dye. *Sustain. Environ. Res.* **2017**, *27* (5), 245−250.

(11) Khodadadi, B.; Bordbar, M.; Nasrollahzadeh, M.; Achillea Millefolium, L. Extract Mediated Green Synthesis of Waste Peach Kernel Shell Supported Silver Nanoparticles: Application of the Nanoparticles for Catalytic Reduction of a Variety of Dyes in Water. *J. Colloid Interface Sci.* **2017**, *493*, 85−93.

(12) Kalita, N. K.; Ganguli, J. N.; Hibiscus Sabdariffa, L. Leaf Extract Mediated Green Synthesis of Silver Nanoparticles and Its Use in Catalytic Reduction of 4-Nitrophenol. *Inorg. Nano-Metal Chem.* **2017**, *47* (5), 788−793.

(13) Talank, N.; Morad, H.; Barabadi, H.; Mojab, F.; Amidi, S.; Kobarfard, F.; Mahjoub, M. A.; Jounaki, K.; Mohammadi, N.; Salehi, G.; Ashrafizadeh, M.; Mostafavi, E. Bioengineering of Green-Synthesized Silver Nanoparticles: In Vitro Physicochemical, Antibacterial, Biofilm Inhibitory, Anticoagulant, and Antioxidant Performance. *Talanta* **2022**, *243* (March), No. 123374.

(14) Ganguli, S.; Howlader, S.; Ullah, A. K. M. A.; Bhuiyan, F. R.; Akhi, A. A.; Hasan, A.; Dey, K.; Islam, S.; Ali, F.; Chakraborty, A. K.; Bhattacharjee, S.; Dey, B. K. Size Controlled Biosynthesis of Silver Nanoparticles Using Ophiorrhiza Mungos, Ophiorrhiza Harrisiana and Ophiorrhiza Rugosa Aqueous Leaf Extract and Their Antimicrobial Activity. *Heliyon* **2023**, *9* (5), No. e16072.

(15) Hileman, J.; Kallstenius, I.; Häyhä, T.; Palm, C.; Cornell, S. Keystone Actors Do Not Act Alone: A Business Ecosystem Perspective on Sustainability in the Global Clothing Industry. *PLoS One* **2020**, *15* (10), No. e0241453.
(16) Haque, M. S.; Nahar, N.; Sayem, S. M. Industrial Water Management and Sustainability: Development of SIWP Tool for Textile Industries of Bangladesh. *Water Resour. Ind.* **2021**, *25*, No. 100145.
(17) Islam, M. M.; Mahmud, K.; Faruk, O.; Billah, S. Assessment of Environmetal Impacts for Textile Dyeing Industries in Bangladesh. In *Proc. Int. Conf. Green Technol. Environ. Conserv. GTEC-2011*; 2011, No. December 2011, 173−181, DOI: 10.1109/GTEC.2011.6167665.
(18) Sharma, P.; Pant, S.; Rai, S.; Yadav, R. B.; Dave, V. Green Synthesis of Silver Nanoparticle Capped with Allium Cepa and Their Catalytic Reduction of Textile Dyes: An Ecofriendly Approach. *J. Polym. Environ.* **2018**, *26* (5), 1795−1803.
(19) Rohaizad, A.; Shahabuddin, S.; Shahid, M. M.; Rashid, N. M.; Hir, Z. A. M.; Ramly, M. M.; Awang, K.; Siong, C. W.; Aspanut, Z. Green Synthesis of Silver Nanoparticles from Catharanthus Roseus Dried Bark Extract Deposited on Graphene Oxide for Effective Adsorption of Methylene Blue Dye. *J. Environ. Chem. Eng.* **2020**, *8* (4), No. 103955.
(20) Sultan, M.; Siddique, M.; Khan, R.; Fallatah, A. M.; Fatima, N.; Shahzadi, I.; Waheed, U.; Bilal, M.; Ali, A.; Abbasi, A. M. Ligustrum Lucidum Leaf Extract-Assisted Green Synthesis of Ultrasound-Assisted Adsorptive Removal of Methylene Blue Dye from Wastewater and Antimicrobial Activity. *Materials (Basel).* **2022**, *15*, 1637.
(21) Singh, J.; Dhaliwal, A. S. Effective Removal of Methylene Blue Dye Using Silver Nanoparticles Containing Grafted Polymer of Guar Gum/Acrylic Acid as Novel Adsorbent. *J. Polym. Environ.* **2021**, *29* (1), 71−88.
(22) Asmare, Z. G.; Aragaw, B. A.; Atlabachew, M.; Wubieneh, T. A. Kaolin-Supported Silver Nanoparticles as an Effective Catalyst for the Removal of Methylene Blue Dye from Aqueous Solutions. *ACS Omega* **2023**, *8*, 480 DOI: 10.1021/acsomega.2c05265.
(23) Alghamdi, Y. G.; Krishnakumar, B.; Malik, M. A.; Alhayyani, S. Design and Preparation of Biomass-Derived Activated Carbon Loaded TiO2 Photocatalyst for Photocatalytic Degradation of Reactive Red 120 and Ofloxacin. *Polymers (Basel).* **2022**, *14* (5), 880.
(24) Cheng, X.; Jiang, D.; Chen, H.; Barati, B.; Yuan, C.; Li, H.; Wang, S. Multi-Stage Adsorption of Methyl Orange on the Nitrogen-Rich Biomass-Derived Carbon Adsorbent: DFT and MD Evaluation. *Chemosphere* **2023**, *338* (June), No. 139218.
(25) Cheng, P.; Wang, X.; Markus, J.; Abdul Wahab, M.; Chowdhury, S.; Xin, R.; Alshehri, S. M.; Bando, Y.; Yamauchi, Y.; Kaneti, Y. V. Carbon Nanotube-Decorated Hierarchical Porous Nickel/Carbon Hybrid Derived from Nickel-Based Metal-Organic Framework for Enhanced Methyl Blue Adsorption. *J. Colloid Interface Sci.* **2023**, *638*, 220−230.
(26) Yuliarto, B.; Septiani, N. L. W.; Kaneti, Y. V.; Iqbal, M.; Gumilar, G.; Kim, M.; Na, J.; Wu, K. C. W.; Yamauchi, Y. Green Synthesis of Metal Oxide Nanostructures Using Naturally Occurring Compounds for Energy, Environmental, and Bio-Related Applications. *New J. Chem.* **2019**, *43* (40), 15846−15856.
(27) Weidner, E.; Karbassiyazdi, E.; Altaee, A.; Jesionowski, T.; Ciesielczyk, F. Hybrid Metal Oxide/Biochar Materials for Wastewater Treatment Technology: A Review. *ACS Omega* **2022**, *7* (31), 27062−27078.
(28) Rahmawati, R.; Kaneti, Y. V.; Taufiq, A.; Sunaryono; Yuliarto, B.; Suyatman; Nugraha; Kurniadi, D.; Hossain, S. A.; Yamauchi, Y. Green Synthesis of Magnetite Nanostructures from Naturally Available Iron Sands via Sonochemical Method. *Bull. Chem. Soc. Jpn.* **2018**, *91* (2), 311−317.
(29) Gowda, S. A. M.; Concepta, L.; Dakshayini, K. Adsorption of Methylene Blue by Silver Nanoparticles Synthesized from Urena Lobata Leaf Extract: Kinetics and Equilibrium Analysis Adsorption of Methylene Blue by Silver Nanoparticles Synthesized from Urena Lobata Leaf Extract: Kinetics and Equilibrium. *Mater. Chem. Phys.* **2022**, *288* (July), No. 126431.
(30) Batool, M.; Daoush, W. M.; Hussain, M. K. Dye Sequestration Using Biosynthesized Silver Nanoparticles Adsorbent in Aqueous Solutions. *Crystals* **2022**, *12* (5), 662.
(31) Banala, R. R.; Nagati, V. B.; Karnati, P. R. Green Synthesis and Characterization of Carica Papaya Leaf Extract Coated Silver Nanoparticles through X-Ray Diffraction, Electron Microscopy and Evaluation of Bactericidal Properties. *Saudi J. Biol. Sci.* **2015**, *22* (5), 637−644.
(32) Azeez, L.; Lateef, A.; Adebisi, S. A.; Oyedeji, A. O. Novel Biosynthesized Silver Nanoparticles from Cobweb as Adsorbent for Rhodamine B: Equilibrium Isotherm, Kinetic and Thermodynamic Studies. *Appl. Water Sci.* **2018**, *8* (1), 1−12.
(33) Ruíz-Baltazar; Á de, J.; Reyes-López, S. Y.; Mondragón-Sánchez; M de, L.; Estevez, M.; Hernández-Martinez, A. R.; Pérez, R. Biosynthesis of Ag Nanoparticles Using Cynara Cardunculus Leaf Extract: Evaluation of Their Antibacterial and Electrochemical Activity. *Results Phys.* **2018**, *11* (August), 1142−1149.
(34) Ajitha, B.; Ashok Kumar Reddy, Y.; Sreedhara Reddy, P. Green Synthesis and Characterization of Silver Nanoparticles Using Lantana Camara Leaf Extract. *Mater. Sci. Eng., C* **2015**, *49*, 373−381.
(35) Stahlová, S.; Slováková, E.; Vaňkátová, P.; Zukal, A.; Kubu°, M.; Brus, J.; Bondarev, D.; Moučka, R.; Sedláček, J. Chain-Growth Copolymerization of Functionalized Ethynylarenes with 1,4-Diethynylbenzene and 4,4′-Diethynylbiphenyl into Conjugated Porous Networks. *Eur. Polym. J.* **2015**, *67*, 252−263.
(36) Martínez, M. T.; Callejas, M. A.; Benito, A. M.; Cochet, M.; Seeger, T.; Ansón, A.; Schreiber, J.; Gordon, C.; Marhic, C.; Chauvet, O.; Fierro, J. L. G.; Maser, W. K. Sensitivity of Single Wall Carbon Nanotubes to Oxidative Processing: Structural Modification, Intercalation and Functionalisation. *Carbon* **2003**, *41* (12), 2247−2256.
(37) Zorn, G.; Liu, L. X - Ray Photoelectron Spectroscopy Investigation of the Nitrogen Species in Photoactive Per Fl Uorophenylazide-Modi Fi Ed Surfaces †. *J Phys Chem C Nanomater Interfaces.* **2014**, *118*, 376−383.
(38) Wei, Z.; Zhou, M.; Qiao, H.; Zhu, L.; Yang, H.; Xia, T. Particle Size and Pore Structure Characterization of Silver Nanoparticles Prepared by Confined Arc Plasma. *J. Nanomater.* **2009**, *2009*, 5−10.
(39) Ahmad, R.; Ansari, K. Fabrication of Alginate@silver Nanoparticles (Alg@AgNPs) Bionanocomposite for the Sequestration of Crystal Violet Dye from Aqueous Solution. *Int. J. Biol. Macromol.* **2022**, *218* (May), 157−167.
(40) Kamath Miyar, H.; Pai, A.; Goveas, L. C. Adsorption of Malachite Green by Extracellular Polymeric Substance of Lysinibacillus Sp. SS1: Kinetics and Isotherms. *Heliyon* **2021**, *7* (6), No. e07169.
(41) Birla, S. S.; Gaikwad, S. C.; Gade, A. K.; Rai, M. K. Rapid Synthesis of Silver Nanoparticles from Fusarium Oxysporum by Optimizing Physicocultural Conditions. *Sci. World J.* **2013**, *2013*, 1.
(42) Foo, K. Y.; Hameed, B. H. Insights into the Modeling of Adsorption Isotherm Systems. *Chem. Eng. J.* **2010**, *156* (1), 2−10.
(43) Inyinbor, A. A.; Adekola, F. A.; Olatunji, G. A. Adsorption of Rhodamine b Dye from Aqueous Solution on Irvingia Gabonensis Biomass: Kinetics and Thermodynamics Studies. *South African J. Chem.* **2015**, *68* (1), 115−125.
(44) Pathania, D.; Sharma, S.; Singh, P. Removal of Methylene Blue by Adsorption onto Activated Carbon Developed from Ficus Carica Bast. *Arab. J. Chem.* **2017**, *10*, S1445−S1451.
(45) Lata, H.; Garg, V. K.; Gupta, R. K. Removal of a Basic Dye from Aqueous Solution by Adsorption Using Parthenium Hysterophorus: An Agricultural Waste. *Dye. Pigment.* **2007**, *74* (3), 653−658.
(46) Ho, Y.; Malarvizhi, R.; Sulochana, N. Equilibrium Isotherm Studies of Methylene Blue Adsorption onto Activated Carbon Prepared from Delonix Regia Pods. *J. Environ. Prot. Sci.* **2009**, *3*, 111−116.
(47) Swamy, M. M.; Nagabhushana, B. M.; Krishna, R. H.; Kottam, N.; Raveendra, R. S.; Prashanth, P. A. Fast Adsorptive Removal of Methylene Blue Dye from Aqueous Solution onto a Wild Carrot

https://doi.org/10.1021/acsomega.3c05992
ACS Omega 2024, 9, 4324−4338

Flower Activated Carbon: Isotherms and Kinetics Studies. *Desalin. Water Treat.* **2017**, *71* (January), 399−405.
(48) Karagöz, S.; Tay, T.; Ucar, S.; Erdem, M. Activated Carbons from Waste Biomass by Sulfuric Acid Activation and Their Use on Methylene Blue Adsorption. *Bioresour. Technol.* **2008**, *99* (14), 6214−6222.
(49) Amuda, O. S.; Olayiwola, A. O.; Alade, A. O.; Farombi, A. G.; Adebisi, S. A. Adsorption of Methylene Blue from Aqueous Solution Using Steam-Activated Carbon Produced from Lantana Camara Stem. *J. Environ. Prot.* **2014**, *5*, 1352−1363.
(50) Akpomie, K. G.; Conradie, J. Biogenic and Chemically Synthesized Solanum Tuberosum Peel−Silver Nanoparticle Hybrid for the Ultrasonic Aided Adsorption of Bromophenol Blue Dye. *Sci. Rep.* **2020**, *10* (1), 1−18.
(51) Jawad, A. H.; Abdulhameed, A. S.; Mastuli, M. S. Acid-Factionalized Biomass Material for Methylene Blue Dye Removal: A Comprehensive Adsorption and Mechanism Study. *J. Taibah Univ. Sci.* **2020**, *14* (1), 305−313.
(52) Low, L. W.; Teng, T. T.; Ahmad, A.; Morad, N.; Wong, Y. S. A Novel Pretreatment Method of Lignocellulosic Material as Adsorbent and Kinetic Study of Dye Waste Adsorption. *Water. Air. Soil Pollut.* **2011**, *218* (1−4), 293−306.
(53) Abuzerr, S.; Darwish, M.; Mahvi, A. H. Simultaneous Removal of Cationic Methylene Blue and Anionic Reactive Red 198 Dyes Using Magnetic Activated Carbon Nanoparticles: Equilibrium, and Kinetics Analysis. *Water Sci. Technol.* **2018**, *2017* (2), 534−545.
(54) Fan, S.; Wang, Y.; Wang, Z.; Tang, J.; Tang, J.; Li, X. Removal of Methylene Blue from Aqueous Solution by Sewage Sludge-Derived Biochar: Adsorption Kinetics, Equilibrium, Thermodynamics and Mechanism. *J. Environ. Chem. Eng.* **2017**, *5* (1), 601−611.
(55) Wang, Y.; Srinivasakannan, C.; Wang, H.; Xue, G.; Wang, L.; Wang, X.; Duan, X. Preparation of Novel Biochar Containing Graphene from Waste Bamboo with High Methylene Blue Adsorption Capacity. *Diam. Relat. Mater.* **2022**, *125* (April), No. 109034.
(56) Wu, M.; Li, Y.; Yue, R.; Zhang, X.; Huang, Y. Removal of Silver Nanoparticles by Mussel-Inspired Fe_3O_4 @ Polydopamine Core-Shell Microspheres and Its Use as Efficient Catalyst for Methylene Blue Reduction. *Sci. Rep.* **2017**, *7*, 42773.
(57) Yuan, N.; Cai, H.; Liu, T.; Huang, Q.; Zhang, X. Adsorptive Removal of Methylene Blue from Aqueous Solution Using Coal Fly Ash-Derived Mesoporous Silica Material. *Adsorpt. Sci. Technol.* **2019**, *37* (3−4), 333−348.
(58) Zhou, S.; Yin, J.; Ma, Q.; Baihetiyaer, B.; Sun, J.; Zhang, Y.; Jiang, Y.; Wang, J.; Yin, X. Montmorillonite-Reduced Graphene Oxide Composite Aerogel (M−rGO): A Green Adsorbent for the Dynamic Removal of Cadmium and Methylene Blue from Wastewater. *Sep. Purif. Technol.* **2022**, *296* (April), No. 121416.
(59) Jawad, A. H.; Mamat, N. F. H.; Abdullah, M. F.; Ismail, K. Adsorption of Methylene Blue onto Acid-Treated Mango Peels: Kinetic, Equilibrium and Thermodynamic Study. *Desalin. Water Treat.* **2017**, *59* (January), 210−219.
(60) Jawad, A. H.; Mallah, S. H.; Mastuli, M. S. Adsorption Behavior of Methylene Blue on Acid-Treated Rubber (Hevea Brasiliensis) Leaf. *Desalin. Water Treat.* **2018**, *124* (September), 297−307.
(61) Jawad, A. H.; Rashid, R. A.; Ishak, M. A. M.; Ismail, K. Adsorptive Removal of Methylene Blue by Chemically Treated Cellulosic Waste Banana (Musa Sapientum) Peels. *J. Taibah Univ. Sci.* **2018**, *12* (6), 809−819.
(62) Jawad, A. H.; Mohammed, S. A.; Mastuli, M. S.; Abdullah, M. F. Carbonization of Corn (Zea Mays) Cob Agricultural Residue by One-Step Activation with Sulfuric Acid for Methylene Blue Adsorption. *Desalin. Water Treat.* **2018**, *118* (September), 342−351.
(63) Amran, F.; Zaini, M. A. A. Sodium Hydroxide-Activated Casuarina Empty Fruit: Isotherm, Kinetics and Thermodynamics of Methylene Blue and Congo Red Adsorption. *Environ. Technol. Innov.* **2021**, *23*, No. 101727.
(64) Abou-Gamra, Z. M.; Medien, H. A. A. Kinetic, Thermodynamic and Equilibrium Studies of Rhodamine B Adsorption By Low Cost. *Eur. Chem. Bull.* **2013**, *2* (7), 417−422.
(65) Girish, C. R.; Murty, V. R. Adsorption of Phenol from Aqueous Solution Using Lantana Camara, Forest Waste: Packed Bed Studies and Prediction of Breakthrough Curves. *Int. Scholarly Res. Not.* **2014**, *2014*, No. 201626, DOI: 10.1155/2014/201626.
(66) Mahmoud, H. R.; Ibrahim, S. M.; El-Molla, S. A. Textile Dye Removal from Aqueous Solutions Using Cheap MgO Nanomaterials: Adsorption Kinetics, Isotherm Studies and Thermodynamics. *Adv. Powder Technol.* **2016**, *27* (1), 223−231.
(67) Adam, F. A.; Ghoniem, M. G.; Diawara, M.; Rahali, S.; Abdulkhair, B. Y.; Elamin, M. R.; Ben Aissa, M. A.; Seydou, M. Enhanced Adsorptive Removal of Indigo Carmine Dye by Bismuth Oxide Doped MgO Based Adsorbents from Aqueous Solution: Equilibrium, Kinetic and Computational Studies. *RSC Adv.* **2022**, *12* (38), 24786−24803.
(68) Tarekegn, M. M.; Balakrishnan, R. M.; Hiruy, A. M.; Dekebo, A. H. Removal of Methylene Blue Dye Using Nano Zerovalent Iron, Nanoclay and Iron Impregnated Nanoclay-a Comparative Study. *RSC Adv.* **2021**, *11* (48), 30109−30131.
(69) Mohammed, N.; Lian, H.; Islam, M. S.; Strong, M.; Shi, Z.; Berry, R. M.; Yu, H. Y.; Tam, K. C. Selective Adsorption and Separation of Organic Dyes Using Functionalized Cellulose Nanocrystals. *Chem. Eng. J.* **2021**, *417* (February), No. 129237.
(70) Devi, T. A.; Ananthi, N.; Amaladhas, T. P. Photobiological Synthesis of Noble Metal Nanoparticles Using Hydrocotyle Asiatica and Application as Catalyst for the Photodegradation of Cationic Dyes. *J. Nanostructure Chem.* **2016**, *6* (1), 75−92.
(71) Taher, M.; Shaari, S. S.; Susanti, D.; Arbain, D.; Zakaria, Z. A. Genus Ophiorrhiza: A Review of Its Distribution, Traditional Uses, Phytochemistry, Biological Activities and Propagation. *Molecules* **2020**, *25* (11), 2611.

https://doi.org/10.1021/acsomega.3c05992
ACS Omega 2024, 9, 4324−4338